Klinkmüller, M., Schreurs, G., Rosenau, M., Kemnitz, H. (2016): Properties of granular analogue model materials: A community wide survey. - *Tectonophysics*, *684*, pp. 23–38.

DOI: http://doi.org/10.1016/j.tecto.2016.01.017

Properties of granular analogue model materials: A community wide survey

Klinkmüller M. [a], Schreurs G [a], Rosenau M. [b], Kemnitz H. [b],

[a] Institute of Geological Sciences, University of Bern, Baltzerstrasse 1+3, CH-3012 Bern. schreurs@geo.unibe.ch, tel. +41 31 631 87 60

[b] Helmholtz−Zentrum Potsdam –Deutsches GeoForschungsZentrum GFZ Telegrafenberg, D-14473 Potsdam, Germany.

Abstract

We report the material properties of 26 granular analogue materials used in 14 analogue modelling laboratories. We determined physical characteristics such as bulk density, grain size distribution, and grain shape, and performed ring shear tests to determine friction angles and cohesion, and uniaxial compression tests to evaluate the compaction behaviour. Mean grain size of the materials varied between c. 100 and 400 μm. Analysis of grain shape factors show that the four different classes of granular materials (14 quartz sands, 5 dyed quartz sands, 4 heavy mineral sands and 3 size fractions of glass beads) can be broadly divided into two groups consisting of 12 angular and 14 rounded materials. Grain shape has an influence on friction angles, with most angular materials having higher internal friction angles (between c. 35° and 40°) than rounded materials, whereas well-rounded glass beads have the lowest internal friction angles (between c. 25° and 30°). We interpret this as an ef-

fect of intergranular sliding versus rolling. Most angular materials have also higher basal friction angles (tested for a specific foil) than more rounded materials, suggesting that angular grains scratch and wear the foil., Most materials have an internal cohesion in the order of 20-100 Pa except for well-rounded glass beads, which show a trend towards a quasi-cohesionless (C <20 Pa) Coulomb-type material. The uniaxial confined compression tests reveal that rounded grains generally show less compaction than angular grains. We interpret this to be related to the initial packing density after sifting, which is higher for rounded grains than for angular grains. Ring-shear test data show that angular grains undergo a longer strain-hardening phase than more rounded materials. This might explain why analogue models consisting of angular grains accommodate deformation in a more distributed manner prior to strain localisation than models consisting of rounded grains.

Introduction

Experimental simulations of brittle deformation of the earth using scaled analogue models have evolved from a qualitative phenomenological approach towards a more quantitative analysis (Ranalli, 2001). Along with this evolution, the number of different granular materials used in analogue modelling experiments has increased (Mandl et al., 1977; Savage and Sayed, 1984; Krantz, 1991; Cobbold and Castro, 1999; Schellart, 2000; Lohrmann et al., 2003; Rossi and Storti, 2003; van Mechelen, 2004; Panien et al., 2006; Rosenau et al., 2009; Graveleau et al., 2011; Gomes, 2013). Granular materials are commonly used in analogue models for simulating upper crustal deformation. In direct comparisons of scaled analogue experiments to test the reproducibility of model results among different physical modelling laboratories, Schreurs et al. (2006, 2015) showed that differences in model materials induce variations in the geometry and evolution of structures. In order to evaluate to what extent the results of physical modelling in tectonics depend on the properties of the model materials and to allow for meaningful quantitative comparisons of model results, it is essential that the physical characteristics and the mechanical behaviour of the materials be determined in a consistent way.

Here, we present an analogue material comparison investigating the properties of dry granular materials from physical modelling laboratories worldwide. In this comparison 14 laboratories participated and a total of 26 granular model materials were analysed using standard methods and apparatuses. We determine the physical characteristics (e.g., density, grain size distribution, and grain shape) and perform ring-shear tests and uniaxial confined compression tests to characterise the mechanical behaviour of each of these materials. We then discuss the implications for comparability of the materials among themselves and their suitability for analogue modelling. All ring-shear and uniaxial confined compression tests were performed by the same person to assure as much as possible a repeatable material handling and filling procedure.

2. Materials

Participating laboratories sent 7 kg of granular material to the Helmholtz Centre Potsdam, German Research Centre for Geosciences (GFZ), where all material tests have been performed. The materials were stored prior to testing for at least one month to acclimatise to the air-conditioned laboratory environment at GFZ. During the measurement periods laboratory temperature and air humidity was 23±2°C and

45 ± 5%, respectively. Each of the tested materials has been assigned an abbreviation with the first three capital letters identifying the laboratory and the last three capital letters designating the type of material.

The granular materials comprise both natural and artificial materials (Table 1; Fig. 1). Natural materials include quartz sands and heavy mineral sands (garnet and zircon sands). Most natural materials are shock heated to eliminate the clay fraction and are sieved to specific grain size distributions by the suppliers. STUSAN and GFZSAN are mixtures of pure quartz sand and a few percent of dyed quartz sand. These "salt'n'pepper" mixtures provide a visual texture that allows monitoring of analogue model deformation using optical correlation techniques (e.g. Adam et al., 2005; 2013). ULISAN is a 1:1 mixture of quartz sand and dyed quartz sand. Artificial materials include corundum sands and glass beads. Brown and white corundum sands consist of aluminium oxides and are produced from reduced melt of high-quality bauxite and pure, mineralised clay, respectively. The glass beads are high-quality vaporised glass spheres. The 26 tested granular materials comprise 14 quartz sands, 5 dyed quartz sands, 4 heavy mineral sands and 3 types of glass beads with different grain size fractions. To distinguish dyed from non-dyed quartz sands, we added “col” (for “coloured”) to the six-letter abbreviation designating the dyed materials.

3. Bulk density, grain size and grain shape

3.1. Density measurements

3.1.1 Measurement method

The bulk density of each granular material was estimated by measuring the mass of a known volume. Material was sifted from a height of 30 cm at a filling rate of c. 250 ml/min into the shear cell of a ring-shear tester (see next section) with known volume. Sifting was done using a sieve structure identical to the one described by Schreurs et al. (2016). Excess material was scraped off to achieve a plane surface.

3.1.2. Results: Density

Bulk densities vary between 1.2 and 1.7 for all granular materials, except for the heavy mineral sands, which have densities between 1.8 and 2.8 g/cm^3 (Table 2).

3.2. Grain size and shape

3.2.1. Grain size analysis

Grain size analysis was performed with a sieve shaker Retsch AS 200 equipped with sieves of 200 mm diameter and six mesh sizes of 63 µm, 125 µm, 224 µm, 355 µm, 400 µm, and 630 µm, yielding five constrained and two unconstrained (<63 µm and >630 µm) grain size classes. Shaking time and amplitude was 4 hours and 3 mm, respectively. Preliminary tests verified these conditions as being effective in separating the grains in typical sands. From an initial charge of 1 kg the maximum material loss was 5 gram (i.e. 0.5 weight-%). The results of the sieve analysis are presented as grain size distribution curves, in which particle grain size is plotted against cumulative weight percentage (Fig. 2).

3.2.2. Results: Grain size and sorting

The tested granular materials are either fine or medium grained sands, with mean grain size (after Folk and Ward, 1957) ranging between 124 and 410 µm, and grain sorting varying from poorly sorted to very well sorted (Table 2). Most materials show a unimodal grain size distribution. The poor sorting of ULISAN col is due to the bi-modal size distribution stemming from mixing dyed and non–dyed quartz sand.

3.2.3 Measurement method: Grain shape

We also quantified the shape of grains using SEM images (Fig. 1) and determined aspect ratio (length ratio of long axis versus short axis), PARIS shape factor (Heilbronner and Keulen, 2006) and SH1 shape factor (Panozzo and Hürlimann, 1983), using the public domain software Image SXM (Barrett, 2002). Differences between PARIS and SH1 grain shape factors are related to how they describe the grains. The PARIS shape factor focuses on indentations of the grain circumference with higher values indicating more indented grains, whereas the SH1 shape factor describes the deviation from perfect circularity of a grain. The two shape factors are defined as follows:

$$PARIS = 2 \times \left(\frac{(P - PE)}{PE} \right) \times 100 \quad \text{and} \quad SH1 = \frac{U^2}{4\pi F}$$

with P = length of original outline, PE = length of outline of convex envelope, U = perimeter of grain, and F = area of grain.

Grain shape and outline were measured and averaged for at least 60 grains of each granular material.

3.2.4 Results: Grain shape

The aspect ratio of the tested granular materials varies between 1.1 and 1.8, the SH1 shape factor ranges from 1.09 to 1.53, and the PARIS shape factor lies between 1.1 and 6.3 (Table 2; Fig. 3). CASSAN, IFPSAN, KYUSAN, TLWSAN, UBESAN and UPUSAN quartz sands have a PARIS shape factor higher than 2.5, with the heavy mineral sands GFZGRS, IFPCSB and IFPCSW having the highest values of 5.2, 5.4 and 6.3, respectively. Overall highly indented materials with a Paris factor > 2.5 show more angular grain shapes than materials with a Paris factor < 2.5. Based on the classification of Powers (1953), we distinguish two broad groups of granular materials (Table 2), "angular" ones (12 materials with predominantly subangular, angular or very angular grains), and "rounded" ones (14 materials with predominantly subrounded, rounded or well-rounded grains). Except for RHUSAN col, all dyed sands have a larger SH1 and PARIS shape factor than their non-dyed equivalents. Whereas dyeing leads to an increase in aspect ratio for NTSAN col, UOPSAN col and ULISAN col, it results in a decrease in aspect ratio for RHUSAN col and GFZSAN col. The three different types of glass beads (GFZGLB) have the lowest SH1 (1.09-1.1) and aspect ratio values (1.1-1.2), and low PARIS values (1.7 or less), and represent the most rounded grains. PARIS values of 2 or less have been determined for GFZSAN, GFZZCS, NTUSAN, RHUSAN, STUSAN, UCPSAN, ULISAN and UPASAN, but these materials have all somewhat higher SH1 and aspect ratio values than glass beads.

4. Mechanical behaviour

4.1. Ring-shear test analysis and results

4.1.1. Ring shear tester setup

The mechanical properties of the granular materials were determined using a Schulze ring-shear tester (Schulze, 1994; Fig. 4), specially designed to measure friction coefficients in loose granular materials accurately at low confining pressures (~0.1 - 10 kPa) and shear velocities (~0.1 – 10 mm/minute) similar to sandbox experiments (Lohrmann et al., 2003). In this tester, the granular material is sheared either against a fixed basal plate (to measure basal friction) or internally (to measure internal friction) at constant normal load and velocity while the shear stress and compaction is measured continuously. In our case we determine the basal friction between a specific granular material and a base covered with "Alkor" foil (since 2012 called "RENOLIT"), a transparent self-adhesive foil that is used in the community to reduce friction along boundary walls. Alkor foil has also been used in analogue benchmarks to standardize the boundary conditions in order to test model reproducibility (Schreurs et al., 2006; 2016). The ring-shear tester consists of a 4 cm high annular shear-cell made of stainless steel holding approximately 0.1 and 1 litre of the material in case of basal and internal measurements, respectively. A ring-shaped-lid is placed onto the filled cell. The lid is counterbalanced by a weight and subjected to a normal force in order to control normal load on the sample. While the cell is rotated, the lid is prevented from rotation by two tie rods connected to a crossbeam (Fig. 4). The force necessary to shear the material is measured continuously. To ensure shearing inside the material and prevent slip between the lid and the granular material, the lid has 20 vanes protruding 4 mm into the material.

Sidewall friction may reduce the normal stress on the actual shear zone and add to the shear stress (silo effect, see Mourgues and Cobbold, 2003), However, these effects are in the order of a few tens of Pa only in the current setup and below the specified testing conditions (>100 Pa).

The physical handling technique used to fill the shear cell is the same as the one used to determine the bulk density, i.e. material was sifted from c. 30 cm into the shear-cell at a filling rate of c. 250 ml/min. Excess material was scraped off carefully to avoid additional compaction and to achieve a plane surface before assembling the shear-cell together with the shear-lid onto the ring-shear testing machine. During ring-shear testing, a shear velocity of 3 mm/min is applied. Sampling rate for all measured parameters (shear load, normal load, shear velocity, and lid displacement) was 50 Hz allowing to accurately detect and if necessary correct for stick-slip behavior.

4.1.2 Qualitative assessment of shear curves

A typical evolution of the shear stress is shown in Figure 5. Shear stress rises from zero to a peak level (peak friction; B in Fig. 5) within the first few millimetres of shear (strain hardening phase) before it drops (strain softening phase) and stabilises after formation of a shear zone (sliding phase) in the material or at the interface between the material and the Alkor foil (dynamic friction; C in Fig. 5). Subsequently the movement of the shear-cell is reversed for a short duration while the normal load is kept constant. Once the shear stress has dropped to zero, the original shear-cell rotation is resumed. Renewed shearing results in a second, similar shear curve whose peak (reactivation friction; D in Fig. 5) is somewhat lower than the first peak. From these curves, three values of friction strengths at the first peak, reactivation peak and on the plateaus are picked manually and assigned peak, reactivation and dynamic friction strength for the applied normal load, respectively. For each granular material, the three values of friction strengths are determined for five different normal loads varying between c. 430 and 2150 Pa. Each normal load step is repeated three times, resulting in a total of 15 measurements for each material.

The strain-hardening phase before the first peak strength (AB in Fig. 5) is followed by a strain-softening phase (BC in Fig. 5) until dynamic strength is reached.

Lohrmann et al. (2003) show that deformation leading to shear zone formation is associated with a sample compaction-decompaction cycle as inferred from volume changes concurrent with the shear stress evolution. The shape of the curve during strain hardening varies for different granular materials and reflects diffuse deformation before the onset of strain localisation.

Fig. 6 shows the shear stress vs. displacement (i.e. the amount of shear strain) curves of an angular granular material (IFPCSW) and well-rounded glass beads (GFZGLB 100-200 µm) for three different normal loads. A comparison of the curves of the two materials at identical normal loads reveals significant differences in the shape of the curves. IFPCSW requires more shear stress to form a shear zone (i.e, it has a higher peak strength) and undergoes more plastic strain prior to failure at peak strength (i.e. has a wider peak) than GFZGLB 100-200 µm. Thus the angular IFPCSW experiences more diffuse deformation prior to shear zone formation than the well-rounded glass beads. The curves after renewed shearing show a similar behaviour, indicating that also prior to shear zone reactivation IFPCSW undergoes more diffuse deformation than the GFZGLB 100-200 µm glass beads.

4.1.3 Quantitative analysis of failure envelopes: friction coefficients and cohesion

We compare two analysis methods to derive friction coefficients and cohesion, and their variability (Fig. 7). We first applied a linear regression of all the normal load vs. shear strength data pairs together (15 data points). This approximates the ideal linear failure envelope in the Mohr stress diagram (Fig. 7a). The slope of the line yields the friction coefficient (μ) and the intercept at zero normal stress gives the cohesion (C).

Because the failure envelopes for granular materials might be non-linear at low normal stresses, i.e. convex (e.g. Schellart, 2000), we introduce an alternative method for deriving friction coefficients and cohesion, which is more sensitive to potential non-linear relationships. This method relies on calculating all possible two point slopes and intercepts for mutually combined pairs of a data set (90 data points) These data are then evaluated through univariate statistics by means of calculating mean and standard deviation and comparing the probability density function to that of a normal distribution (Fig. 7b). Usually the peaks of the experimental probability density function are close to or narrower than a normal distribution. This suggests that the calculated standard deviation is a conservative value for variability compared to the very small, and likely not representative variability resulting from applying a linear regression to the whole data set at once.

For the datasets presented here, we found no significant differences between the two analysis methods, indicating linear failure envelopes for all granular materials for normal stresses in the range from 430 to 2150 Pa. The values determined are given in Tables 3 and 4. From the friction coefficients, we derive the friction angles, which correspond to $\tan^{-1}\mu$ (Fig. 8 and 9; Table 3 and 4).

Results: Internal friction angles and internal cohesion

For all but two granular materials the angle of internal peak friction is systematically higher than the angle of internal reactivation friction by 1-8°, while the angle of internal reactivation friction is in turn 3-10° higher than the angle of internal dynamic friction (Fig. 8a). The two exceptions are the dyed sands NTUSAN col and UOPSAN col. Internal peak friction angles vary between 33° and 39° for quartz sands, between 31° and 40° for dyed quartz sands, and between 35° and 37° for heavy mineral sands. Glass beads have the lowest angles of internal peak friction varying between 26° and 30°.

Internal reactivation friction and internal dynamic friction angles for all materials range from 24° to 36° and from 22 to 35°, respectively, with glass beads having once again the lowest angles, ranging from 24° to 26° and from 22° to 24°, respectively (Fig. 8a). For the three types of glass beads, the internal friction angle increases with mean grain size.

Extrapolated cohesion values vary considerably, ranging from 1 to 134 Pa at internal peak friction, from 25 to 119 Pa at internal reactivation friction, and from 26 to 107 at internal dynamic friction (Fig. 8b). The standard deviation is in most cases higher than the cohesion value itself, suggesting that the cohesion values should be considered as “very approximate”. For 18 out of 26 materials, the internal cohesion is highest at reactivation friction. Also for 18 out of 26 materials, cohesion is lowest at internal peak friction, with all three types of glass beads and four quartz sands, IFPSAN, KYUSAN, NTUSAN and UBESAN having values below 25 Pa.

Results: Basal friction angles and basal cohesion

The basal friction angles of granular materials on Alkor foil show similar systematics as for the internal friction angles, i.e. the basal peak friction angle of a specific material is higher than its basal reactivation friction angle, which in turn is higher than the basal dynamic friction angle (Fig. 9a). Exceptions are RHUSAN, ULISAN, and the dyed NTUSAN col, ULISAN col and UOPSAN col. All but five materials have basal peak friction angles between 18° and 26°, with only RHUSAN, ULISAN, ULISAN col and the three glass beads having basal peak friction angles below 17°. For quartz sands the angles of basal peak friction, basal reactivation friction and basal dynamic friction vary between 15°- 22°, 11° - 20°, and 12° - 19°, respectively; for dyed quartz sands between 16° - 22°, 14° - 25°, and 13° – 19°, respectively; for heavy mineral sands between 25° - 26°, 23° - 25°, and 22 - 25°, respectively, and for glass beads between 14° - 17°, 12° - 15°, and 12 – 15°, respectively.

Inferred basal cohesion values are overall higher than the internal cohesion values, with nearly all materials having a cohesion higher than 100 Pa (Fig. 9b). Exceptions are the three glass beads and the dyed UOPSAN col, which have cohesion values below 100 Pa. In 11 out of 26 materials cohesion is lowest at basal peak friction, and in 16 out of 26 materials cohesion is largest at basal reactivation friction.

4.2. *Uniaxial confined compression test analysis and results*

4.2.1. Uniaxial tester setup

We performed uniaxial confined compression tests in order to get proxies for the compaction behaviour and the elasticity of the granular materials. The uniaxial confined compression tester comprises a steel jar (80 mm in diameter, 85 mm in height), in which sample material is compressed uniaxially via a servo-controlled piston in the vertical direction. The filling procedure is identical to the one used for the ring-shear tester. The jar is stiff enough (10 mm thick steel walls) to prevent the sample from deforming laterally and its inner walls are polished in order to minimize sidewall friction. Uniaxial shortening was applied at a rate of 5 x 10^{-7} s^{-1} until maximum loading at 2000 kPa is reached, followed by unloading at the same rate. Uniaxial compression in the vertical direction was measured at a frequency of 20 Hz using a stress sensor with a resolution of c. 100 Pa. A complete compression test encompassed 50 loading-unloading cycles.

4.2.2 Qualitative assessment of uniaxial stress-strain curves

All stress-strain curves derived from the uniaxial tester were non-linear and involved small amounts of initial settling of machine parts, followed by permanent and elastic strains during loading and unloading. The first loading-unloading cycles (Fig. 10) were strongly concave upward and mainly caused compaction of the bulk volume with more than 50% of the total strain in this cycle (typically 0.1 – 1%) not recovered after unloading. Until the last of the 50 loading-unloading cycles, the non-linearity of the stress-strain curves decreases exponentially (not shown here) with compaction of the bulk volume decreasing to less than 10% of the total strain in the last cycle. Thus, the stress-strain curves derived during early cycles reflect mainly the process of compaction, whereas the stress-strain curves derived during late cycles converge towards the elastic behaviour of the bulk sample material.

4.2.3 Semi-quantitative analysis of compaction behaviour and elasticity

As a measure of compaction we report the total compaction after the 50th loading cycle ,C_t, and a compaction index C_i using the following equation:

$$C_i = eps_1 / eps_{50}$$

with eps_1 and eps_{50} indicating the non-recoverable strain after the first and fiftieth loading cycle, respectively. C_t represents the relative amount of compaction gained in the first loading cycle and therefore scales with the ability of the material to compact. Although the maximum load (2000 kPa) and the number of loading cycles (50) far exceed typical analogue modelling experimental conditions, this method provides a quantitative measure of the compaction behaviour of the material, which should correlate with diffuse deformation observed in sandbox experiments.

As outlined above the sample response to uniaxial strain converges towards elastic behaviour after 50 loading-unloading cycles. To get a quantitative measure of the elastic behaviour, we use the slope of the 50^{th} loading curve fitted by a line (Fig. 10). As the slope of the line relates applied stress to strain and has the unit of stress, it is an elastic modulus. It can be described as the axial stress-strain ratio at zero lateral strain K_0. In the further text we refer to this parameter as the elastic modulus K_0.

Based on multiple iterations of compression tests on GFZSAN and UBESAN a precision of 0.2% and 7% has been assigned to total compaction and compaction index measurements, respectively, and a precision of 10% to K_0 measurements. Since compaction and sidewall friction take up part of the applied stresses in all cycles, however, the inaccuracy of K_0 measurements may be as high as 30%.

Results: Compaction and elasticity

Total compaction, C_t, varies from 0.6% to 6.9% in the samples (Fig. 11, Table 5), with angular materials showing a tendency for higher C_t values than rounded materials. Glass beads and rounded, non-dyed quartz sands have C_t values between 0.6 and 1.4%. Dyed quartz sands compact more than their non-dyed equivalents with total compaction values ranging from 1.4 to 6.9% (Table 5)

The relative compaction index, C_i, ranges between 32% and 65%, indicating that independent of total compaction, all materials initially compact in a rather similar way with 1/3 to 2/3 of the total compaction occurring in the first cycle.

K_0 for all materials ranges from 639 to 1829 MPa, which is about 1-2 orders of magnitude lower than the elastic moduli (e.g. G, K,…) of the respective mineral or rock framework they would constitute (e.g. 10-100 GPa for sandstone). There is an overall increase of K_0 with increasing bulk density (Table 5; Fig. 11), with heavy mineral sands GFZGRS, GFZZCS and IFPCSB having the highest values.

5. Discussion

5.1 Comparison of ring-shear test results with previously published data

5.1.1 Limits of comparability

A direct comparison of our ring-shear test results with previously published data is hindered by the fact that past studies partly applied different test procedures and partly used different handling and filling techniques (Mandl et al., 1977; Krantz, 1991; Schellart, 2000; Lohrmann et al., 2003; Panien et al., 2006; Gomes, 2013).

Test procedures used

Krantz (1991), Schellart (2000), and Lohrman et al. (2003) used a Hubbert-type shear-box (Hubbert, 1951), but the design of these shear-boxes varied considerably. Krantz (1991) and Schellart (2000) moved a hanging ring above a stationary ring to initiate a shear zone, whereas Lohrmann et al. (2003) used a box on wheels, provoking additional friction by resistance to rolling of the wheels or by rolling of the wheels over sand grains.

Handling techniques

Krantz (1991) demonstrated that the physical handling technique used to fill the shear cell has a large influence on material density and on the mechanical properties, notably on the friction angles. Pouring of dry quartz sand in the shear cell resulted in a lower density (1.53 g/cm^3) than sifting of the same quartz sand (1.75 g/cm^3), and shear tests revealed that internal peak friction angles increased with increasing density (Krantz, 1991). Lohrmann et al. (2003) arrived at similar conclusions showing that internal peak friction angles for dry poured sands were between 4° and 12° lower than for dry sifted sands, with fine-grained sands showing larger differences than coarse-grained sands.

Ring-shear tests by Lohrmann et al. (2003), Panien et al. (2006) and Gomes (2013) confirmed the difference in rheological behaviour between sifted and poured sands. Gomes (2013) suggested that the two filling techniques also produce differences in cohesion, with values of cohesion at internal peak strength for poured quartz sands more than twice as high (c. 110-140 Pa) as those for sifted quartz sands. However, in tests by Krantz (1991) and Lohrmann et al. (2003) the differences in cohesion for sifted and poured sands are less clear and in some cases poured sands have lower cohesion values than sifted sands. Gomes (2013) also tested the influence of filling height and only found minimal differences of 1-2° in internal peak friction angles for quartz sands sifted or poured from either 20 or 10 cm height.

5.1.2. Effect of grain shape

The handling technique used by Panien et al. (2006) to fill the ring-shear tester involved sifting granular materials from a height of 30 cm at a filling rate of c. 200 cm^3/min corresponds closely to the handling technique used in this study. Tested materials such as quartz sands, corundum sands and glass fragments showed internal friction angles comparable to those determined in this study, with angles of internal peak friction, internal reactivation friction and internal dynamic friction ranging from 36° to 42°, from 33° to 37°, and from 31 to 35°, respectively (Panien et al., 2006). Corresponding inferred cohesion values varied between c. 5 and 100 Pa. As in our study, ring-shear testing of well-rounded and highly spherical microbeads yielded much lower friction angles with values of 22°, 22° and 21° at internal peak, internal reactivation and internal dynamic friction, respectively (Panien et al., 2006). Schellart (2000), who used a Hubbert-type shear box and poured sand from 10 cm height, found that internal peak friction angles and cohesion are mainly dependent on grain shape (rounding and sphericity) with, for example, well-rounded, highly spherical glass microspheres with grain sizes between 90 and 180 mm having lower cohesion and internal peak friction angles than (sub-) angular quartz sands with identical grain sizes.

Shear tests on dense quartz sands by Krantz (1991) using a Hubbert-type shear box indicated that internal friction angles for shear zone reactivation are essentially the same as for shear zone initiation (at peak strength), and that shear zone reactivation is accompanied by a significant drop in cohesion (c. 300 Pa). These observations are not in agreement with our ring-shear tests, which show that internal reactivation friction angles are systematically lower than internal peak friction angles, and that cohesion values are generally somewhat higher for shear zone reactivation. These discrepancies are possibly related to differences in test procedure and handling technique.

5.2 Property dependencies of granular materials

In order to check for interdependencies of granular material properties, we cross-correlated our data. A subset of our data is shown in Fig 12, whereas cross-correlation of all ring-shear test data is given in Appendix 1. Points are plotted in red if the correlation is significant at the 95% level based on the Pearson correlation coefficient. Apart from correlations within generic groups (i.e. grain shape analysis data, uniaxial confined compression test data and ring-shear test data; for the latter see also Appendix 1), relevant and interpretable correlations exist between grain shape parameters and friction coefficients, between total compaction and internal friction coefficients, and between K_0 and density.

5.2.1 Effects of grain shape

Grain shape effects on internal friction: rolling vs. sliding

Grain shape clearly has an influence on internal friction angles, with angular materials generally having higher friction angles than rounded materials. Well-rounded glass beads showing the lowest aspect ratios and SH1 shape factors, and rather low PARIS shape factors have the lowest internal friction angles. The lower internal friction angle of rounded materials is most likely due to the fact that rounded grains preferentially roll instead of slide against each other (Mair et al., 2003; Desrues and Viggiani, 2004).

Grain shape effects on compaction behaviour: initial packing density

Grain shape also affects the total compaction as observed in the uniaxial confined compression tests with angular grains generally showing more total compaction than rounded grains. The difference in compaction behaviour between the two types of materials is also evident from an analysis of the stress-strain curves derived from the ring-shear tests. Not only do angular materials require more shear stress until failure at peak strength than well-rounded materials, and consequently, angular materials will have higher peak friction angles, but they also undergo more plastic strain prior to failure. This indicates that angular materials undergo more diffuse deformation than rounded materials. This diffuse deformation is associated with sample compaction and decompaction (i.e., dilation) during pre-failure deformation. Lohrmann et al. (2003) showed that failure at peak strength corresponds to the maximum decompaction rate. Angular materials will thus initially compact more than rounded grains and hence subsequently need to undergo more decompaction (dilation) in order for grains to be able to move and slide past each other to form a dilatant shear zone.

We speculate that this behaviour is related to the initial packing density of the material after sifting: For identical sifting procedures (i.e. sifting rate and height) rounded grains may arrange more easily into a dense packing while angular grains tend to get stuck in a less preferential configuration. In that way, the effect of grain shape is similar to the effect of handling technique (i.e. sifting vs. pouring).

Grain shape effects on shear zone reactivation

The ease of reactivation of an already existing shear zone also seems to be dependent on grain shape. Angular granular materials show higher angles of internal reactivation friction than more rounded quartz sands and particularly when compared to glass beads. Schulze (2008) suggests that decreasing the shear stress to zero after a shear zone has formed, with constant normal load still applied, causes the bulk material to relax enabling slight rearrangements of the grain structure, particularly in the shear zone, which has undergone dilation. Thus a reactivation needs to partly re-establish the dilatant zone (i.e. the shear zone), which will require more shear stress for angular grains than for rounded grains.

Grain shape effects on basal friction: scratching the walls

The three different grain sizes of well-rounded glass beads clearly represent the granular materials with the lowest internal friction angles in the present data set (Fig. 8a; Table 3). However, this distinction from the remaining materials becomes less prominent when basal friction is considered (Fig. 9a; Table 4). The basal friction angles of glass beads are more similar to the ones determined for rounded quartz sands, such as RHUSAN and ULISAN This might indicate that rolling of well-rounded glass beads is less effective when glass beads are sheared along the Alkor foil than when glass beads are internally sheared, and consequently the difference in basal friction angles with other rounded materials decreases.

Most angular materials have higher basal friction values than rounded materials, in particular with respect to the glass beads (Fig. 9; Table 4). We suggest that this difference is caused by the tendency of angular grains to cut more easily into the Alkor foil than rounded grains. Similar dynamics are to be expected for angular grains moving along other wall materials such as plastic and wood (Panien et al., 2006), This suggests that the use of angular grains favours tear and wear of model walls, and that scratched walls or foils should be exchanged to minimize the influence of boundary friction on the model results.

Grain shape effects on cohesion

Grain shape seems to have an effect also on cohesion as aspect ratio correlates positively with cohesion (Fig. 12). This is exemplified by well-rounded glass beads, which are amongst the least cohesive materials tested (Fig. 8b). However, we cannot discern whether the low cohesion of glass beads is shape controlled (balls have the smallest possible contact areas) or material controlled (e.g. by the susceptibility to electrostatic loads).

For each granular material, except UPOSAN col, basal cohesion values at peak, reactivation and dynamic friction are systematically higher than the corresponding internal cohesion values, suggesting an influence of the Alkor foil on cohesion.

Internal and basal cohesion values are nearly always higher for shear zone reactivation than for shear zone initiation at peak strength (Fig. 8b, 9b). The difference can be explained by the ring-shear test procedure. Before renewed shearing is applied to determine reactivation strength, the shear stress is reduced to zero. It can be expected that during this relaxation phase, grains move closer together and the grain contact area increases, resulting in an increase in cohesion in the shear zone especially if grain size is heterogeneous. As the required shear stress to achieve reactivation strength is less than for peak strength, comparatively less decompaction will occur resulting in a higher residual cohesion at reactivation strength.

5.2.2 Effects of dyeing

Dyeing a granular material changes its physical properties, generally decreasing its bulk density and sorting, and changing the shape of the grains, resulting in higher aspect ratios, SH1 and PARIS factors. However, the influence of dyeing on the mechanical behaviour is difficult to assess. For some sands dyeing results in higher internal friction angles, for other sands in lower internal friction angles. Similarly, some sands show a higher cohesion after dyeing, others a lower cohesion. The non-systematic changes in mechanical behaviour might be related to differences in the nature of the dyeing material and the applied dyeing procedure.

5.2.3 Role of material stiffness

The observed dependency of K_0 on density relates to a common specific modulus, i.e. a constant ratio of K_0 and density, of the materials tested. Since all materials are composed of grains of minerals, the existence of such a common specific modulus seems intuitively straightforward. The high stiffness of the bulk materials tested indicates that elastic strain under typical experimental conditions is generally small (nanometer scale deformation) and below the detection threshold of state-of-the-art monitoring techniques (e.g. particle interference velocimetry measurement systems). Any observable (> micrometer scale) distributed deformation in sandbox models therefore can be attributed to diffuse plastic strain and associated compaction/decompaction.

Conclusions

We tested 26 granular analogue materials from 14 analogue modelling laboratories. We determined physical characteristics, such as density, grain shape and grain size distribution, as well as mechanical properties including, internal and basal friction angles, cohesion, elasticity and compaction behaviour. It is emphasised that all mechanical tests were done by the same person at constant air conditioned laboratory conditions (23°C and 45% relative humidity). For all mechanical tests we used a specific handling technique (sifting from 20 cm height at a rate of 250 ml/min). From a comparison of the tested granular materials, the following conclusions can be drawn:

1. Grain shape has an influence on friction angles, with angular materials generally having higher internal peak friction angles (between c. 35° and 40°) than more rounded materials, with well-rounded glass beads having the low-

est internal friction angles (between 25° and 30°). This effect can be attributed to the ability of rounded grains to roll instead of to slide.

2. The effect of mean grain size and grain size distribution on friction angles is difficult to assess. When considering quartz sands and heavy mineral sands, there seems to be no clear relationship between mean grain size and friction angle. The three size fractions of glass beads show an increase in internal friction angles with increasing mean grain size.
3. Most angular materials also have higher basal friction angles than more rounded quartz sands and glass beads, suggesting that angular grains scratch and wear the Alkor foil more easily than rounded grains.
4. Angular materials mostly show higher angles of internal reactivation friction than rounded materials, particulary when compared to glass beads.
5. In the ring-shear tests angular materials show a longer strain hardening phase than more rounded materials indicating that the former ones undergo more diffuse deformation, i.e. more compaction and decompaction prior to shear zone formation. Such a shape effect on compaction is also evident from uniaxial compaction tests and can be related to the less dense packing of sifted angular materials compared to sifted round materials.
6. Dyeing granular materials influences the mechanical properties, but affects internal and basal friction angles, as well as cohesion in a non-systematic way.
7. Although inferred cohesion values have large uncertainties and scatter widely, most non-dyed granular materials have an internal cohesion between 20 and 100 Pa. The fact that well-rounded glass beads have lower internal cohesion values and trend towards a near cohesionless Coulomb behaviour at peak friction indicates that grain shape also has an influence on cohesion.

This effect might be related to smaller contact areas of round grains compared to angular grains and/or their susceptibility to electrostatic loads.

8. Basal cohesion values of the granular materials on Alkor foil are systematically higher than internal cohesion values, suggesting an effect of the foil on cohesion.
9. Values of internal and basal cohesion at shear zone reactivation are nearly always higher than internal and basal cohesion at shear zone formation (peak friction).
10. Elastic deformation of materials tested here is at the nanoscale and is not observable with current monitoring techniques.

Acknowledgments

Funding by Swiss National Foundation (SNF No 200020-122143 and No 200020-109320) is gratefully acknowledged. We thank all participating laboratories for sending samples of their granular materials, Rüdiger Kilian for discussions on grain shape analysis, and Vincent Strak and an anonymous reviewer for helpful comments and suggestions on an earlier version of this paper.

References

Adam, J., Urai, J., Wienecke, B., Oncken, O., Pfeiffer, K., Kukowski, N., Lohrmann, J., Hoth, S., Van Der Zee, W., Schmatz, J., 2005. Shear zone formation and strain distribution in granular materials – new insights employing high-resolution optical image correlation. Journal of Structural Geology 27, 283-301.

Adam, J., Klinkmüller, M., Schreurs, G., Wieneke, B. 2013. Quantitative 3D strain analysis in analogue experiments simulating tectonic deformation: Integration of X-ray computed tomography and digital volume correlation techniques. Journal of Structural Geology 55, 127-149.

Barrett, S.D., 2002. Software for Scanning Microscopy. Proceedings of the Royal Microscopical Society 37/3, 167-174.

Cobbold, P.R. and Castro, L. 1999. Fluid pressure and effective stress in sandbox models. Tectonophysics 301, 1-19.

Desrues, J., Viggiani, G., 2004. Strain localization in sand: an overview of the experimental results obtain in Grenoble using stereophotogrammetry. International Journal for Numerical and Analytical Methods in Geomechanics 28, 279-321.

Folk, R.L., Ward, W.C., 1957. Brazos river bar: a study in the significance of grain size parameters. Journal of Sedimentary Petrology 27 (1), 3-26.

Forsyth, A.J., Hutton, S., Rhodes, M.J., 2002. Effect of cohesive interparticle force on the flow characteristics of granular material. Powder Technology 126 (2), 150–154.

Gomes, C.J.S. 2013. Investigating new materials in the context of analog-physical models. Journal of Structural Geology 46, 158-166.

Graveleau, F., Hurtrez, J.-E., Dominguez, S., and Malavieille, J. 2011. A new experimental material for modelling relief dynamics and interaction between tectonics and surface processes. Tectonophysics 513, 68-87.

Heilbronner, R., Keulen, N., 2006. Grain size and grain shape analysis of fault rocks. Tectonophysics 427, 199-216.

Hubbert, M. K., 1951. Mechanical basis for certain familiar geologic structures. Geological Society of America Bulletin 62, 1259-1273.

Krantz, R.W., 1991. Measurements of friction coefficients and cohesion for faulting and fault reactivation in laboratory models using sand and sand mixtures. Tectonophysics 188, 203-207

Lohrmann, J., Kukowski, N., Adam, J., Oncken, O., 2003. The impact of analogue material properties on the geometry, kinematics and dynamics of convergent sand wedges. Journal of Structural Geology 25, 1961-1711.

Mair, K., Frye, K.M., Marone, C., 2002. Influence of grain characteristics on the friction of granular shear zones. Journal of Geophysical Research 107 (B10), 4/1-4/9.

Mandl, G., de Jong, L.N.J., Maltha, A., 1977. Shear zones in granular material. Rock Mechanics 9, 95-144.

Mechelen, J.L.M. van, 2004. Strength of moist sand controlled by surface tension for tectonic analogue modelling. Tectonophysics 384, 275-284.

Mourgues, R., Cobbold, P.R., 2003. Some tectonic consequences of fluid overpressures and seepage forces as demonstrated by sandbox modelling. Tectonophysics, 376, 75-97.

Panien, M., Schreurs, G., Pfiffner, A., 2006. Mechanical behaviour of granular materials used in analogue modelling: insights from grain characterisation, ring-shear tests and analogue experiments. Journal of Structural Geology 28, 1710-1724.

Panozzo, R., Hürlimann, H., 1983. A simple method for the quantitative discrimination of convex and convex-concave lines. Microscopica Acta 87 (2), 169-176.

Powers, M.C. 1953. A new roundness scale for sedimentary particles. Journal of Sedimentary Petrology 23, 117-119.

Ranalli, G., 2001. Experimental tectonics: from Sir James Hall to the present. Journal of Geodynamics 32(1-2), 65-76.

Rosenau, M., Lohrmann, J., and Onno O., 2009. Shocks in a box: An analogue model of subduction earthquake cycles with application to seismotectonic forearc evolution. Journal of Geophysical Research 114, B01409.

Rossi, D. and Storti, F. 2003. New artificial granular materials for analogue laboratory experiments: aluminum and siliceous microspheres. Journal of Structural Geology 25, 1893-1899.

Savage, S.B., Sayed M., 1984. Stresses developed by dry cohesionless granular materials sheared in an annular shear cell. Journal of Fluid Mechanics 142, 391-430.

Schellart, W.P., 2000. Shear test results for cohesion and friction coefficients for different granular materials: scaling implications for their usage in analogue modelling. Tectonophysics 324, 1-16.

Schreurs, G., Buiter, S.J.H., Boutelier. J., Burberry, C., Callot, J.-P., Cavozzi, C., Cerca, M., Chen, J.-H., Cristallini, E., Cruden, A.R., Cruz, L., Daniel, J.-M., Da Poian, G., Garcia, V.H., Gomes, C.J.S., Grall, C., Guillot, Y., Guzmán, C., Hidayah, T.N., Hilley, G., Klinkmüller, M., Koyi, H.A., Lu, C.-Y., Maillot, B., Meriaux, C., Nilfouroushan, F., Pan, C.-C., Pillot, D., Portillo, R., Rosenau, M., Schellart, W.P., Schlische, R.W., Take, A., Vendeville, B., Vergnaud, M. Vettori, M., Wang, S.-H., Withjack, M.O., Yagupsky, D., Yamada, Y. 2016. Benchmarking analogue models of brittle thrust wedges. Journal of Structural Geology, in revision.

Schreurs, G., Buiter, S.J.H., Boutelier, D., Corti, G., Costa, E., Cruden, A., Daniel, J.-M., Hoth, S., Koyi, H., Kukowski, N., Lohrmann, J., Ravaglia, A., Schlische, R.W., Withjack, M.O., Yamada, Y., Cavozzi, C., DelVentisette, C., Elder Brady, J., Hoffmann-Rothe, A., Mengus, J.-M., Montanari, D., Nilforoushan, F., 2006. Analogue benchmarks of shortening and extension experiments. In: Buiter, S.J.H., Schreurs, G. (Eds), Analogue and Numerical Modelling of Crustal-Scale Processes. Geological Society, London, Special Publication 253, 1-27.

Schulze, D., 1994. Entwicklung und Anwendung eines neuartigen Ringschergerätes. Aufbereitungstechnik 35 (10), 524-535.

Schulze, D., 2008. Pulver und Schüttgüter – Fließeigenschaften und Handhabung. Springer Berlin.

Figures

Fig. 1. SEM photographs of tested granular materials. Length of white scale bar in each photograph is 500 μm.

Fig. 2. Grain size classes plotted against cumulative weight.

Fig. 3. Grain shape analysis using aspect ratio, and SH1 shape and PARIS factors. Angular granular materials are indicated in bold italics, rounded materials in normal font.

Fig. 4. Ring-shear tester (after Schulze, 1994).

Fig. 5. Example of shear stress curves at different normal loads, AB = strain hardening part of curve, BC = strain softening part of curve, B = peak strength, C = dynamic strength, and D = reactivation strength.

Fig. 6. Shear stress plotted as a function of cell displacement (~ the amount of shear strain) for angular quartz sand (IFPCSW) and well-rounded glass beads (GFZGLB 100-200 μm) for three different normal loads.

Fig. 7. Example of ring-shear test data analysis (UBESAN, internal) (a) Linear regression analysis of shear strength vs normal load data pairs (15 data). (b) Histograms of friction co-efficients and cohesion derived from mutual two-point regression analysis (90 data).

Fig. 8. Internal friction angles and cohesion values (a) Angles of internal peak friction, inter-nal reactivation friction and internal dynamic friction. (b) Extrapolated cohesion values at internal peak friction, internal reactivation friction and internal dynamic friction. Angular granular materials are indicated in bold italics, rounded materials in normal font.

Fig. 9. Basal friction angles and cohesion values (a) Angles of basal peak friction, basal re-activation friction and basal dynamic friction. (b) Extrapolated cohesion values at basal peak friction, basal reactivation friction and basal dynamic friction. Angular granular materials are indicated in bold italics, rounded materials in normal font.

Fig. 10. Uniaxial confined compression test after the first and 50th cycle. First loading – unloading cycle is dominated by compaction; later cycles represent more elastic behaviour. The elastic modulus, K_0, is determined at the 50th cycle along loading path (dashed line).

Fig. 11. Values of bulk density, compaction index (left scale), total compaction and elastic modulus, K_0, (right scale). Angular granular materials are indicated in bold italics, rounded materials in normal font.

Fig. 12. Bivariate cross-correlation matrix of selected data. Points are plotted in red if the correlation is significant at the 95% level based on Pearson correlation coefficient. Apart from correlations within generic groups (shape and grain size analysis, uniaxial confined compression tests and ring shear test data), relevant and interpretable correlations exist between shape parameters and friction parameters as well as between K_0 with density and total compaction with internal friction. C is cohesion, C_i is compaction index, C_t is total compaction, K_0 is the elastic modulus, μ is coefficient of friction with subscripts "peak", "dyn" and dynbas" indicating coefficients of peak internal friction, dynamic internal friction and dynamic basal friction, respectively.

Tables

Table 1. Overview of tested granular materials with details on origin, composition and supplier. First three capital letters in third column identify the participating institute: CAS = Czech Academy of Sciences, GFZ = German Research Centre for Geosciences, IFP = IFP Energies nouvelles, KYU = Kyoto University, NTU = National Taiwan University, RHU = Royal Holloway University, STU = Stanford University, TLW = TecLab Wroclaw, UBE = University of Bern, UCP = Université de Cergy Pontoise, ULI = Université Lille, UOP = Universidade Federal de Ouro Preto, UPA = Università degli studi di Parma, UPU = Uppsala University,

UTO = University of Toronto. Last three capital letters in third column identify the type of granular material: CSB = corundum sand brown, CSW = corundum sand white, GLB = Glass beads, GRS = garnet sand, SAN = quartz sand, ZCS = zircon sand.

Table 2. Physical characteristics of tested granular materials. Note that the mean grain size of GFLGLB 300-400 mm is larger than the maximum grain size indicated by the supplier. P = poorly sorted, M = moderately sorted, MW = moderately to well sorted, W = well sorted, VW = very well sorted.

Table 3. Internal friction coefficients, internal friction angles and cohesion values. Internal friction angles are rounded to the nearest integer. Angular granular materials are indicated in bold italics, round materials in normal font.

Table 4. Basal friction coefficients, basal friction angles and cohesion values. Basal friction angles are rounded to the nearest integer. Angular granular materials are indicated in bold italics, round materials in normal font.

Table 5. Bulk density, elastic modulus K_0, total compaction (C_t) and compaction index (C_i.)

Appendix

Appendix 1. Bivariate cross-correlation matrix of internal and basal friction data. C is cohesion, μ is coefficient of friction; subscripts “peak”, “reac” and “dyn” indicate respective values at internal peak, internal reactivation and internal dynamic conditions, respectively; subscripts “peakbas”, “reacbas” and “dynbas” indicate respective values at basal peak, basal reactivation and basal dynamic conditions, respectively.

836

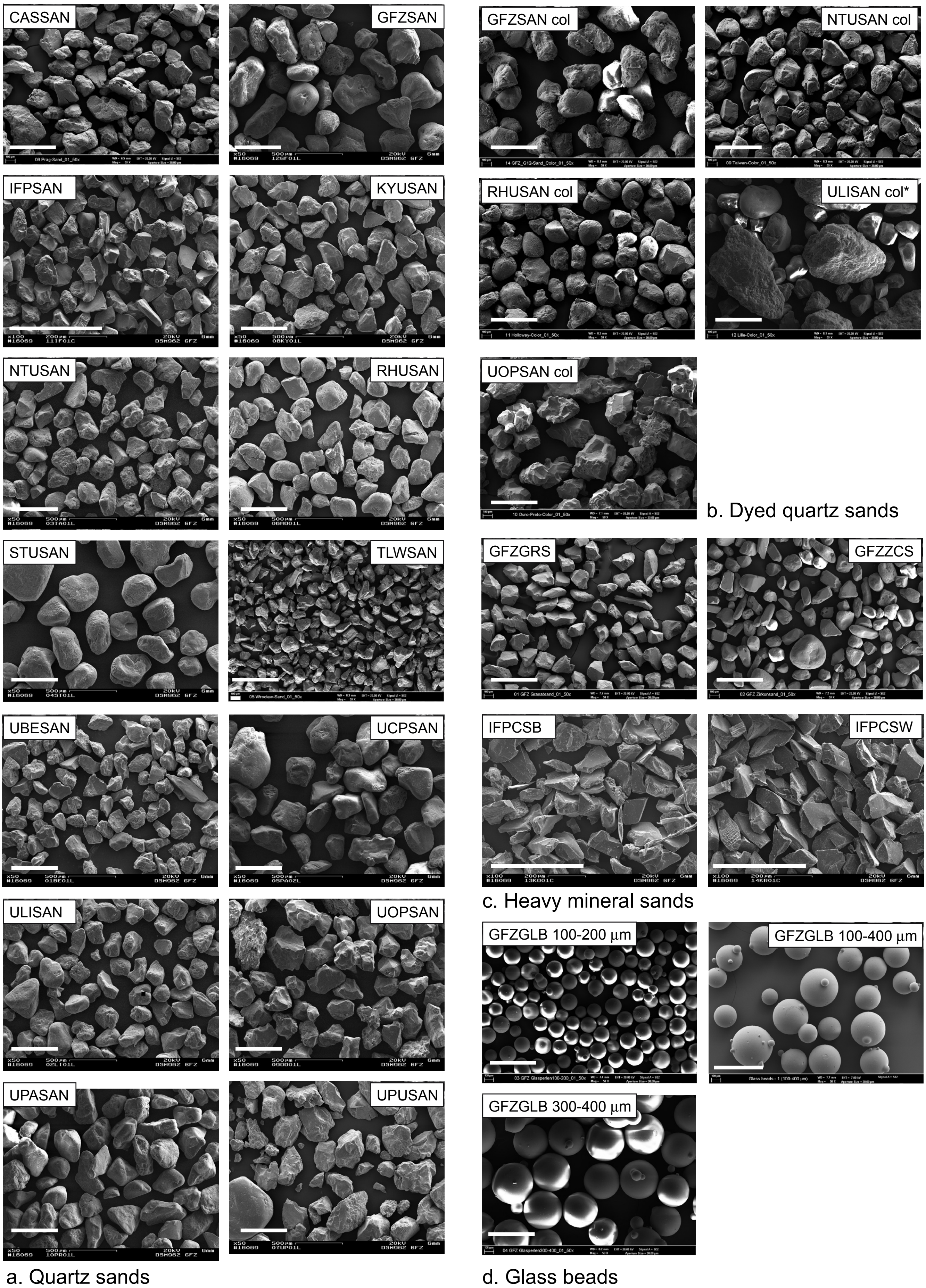

Fig. 1. SEM photographs of tested granular materials. Length of white scale bar in each photograph is 500 μm

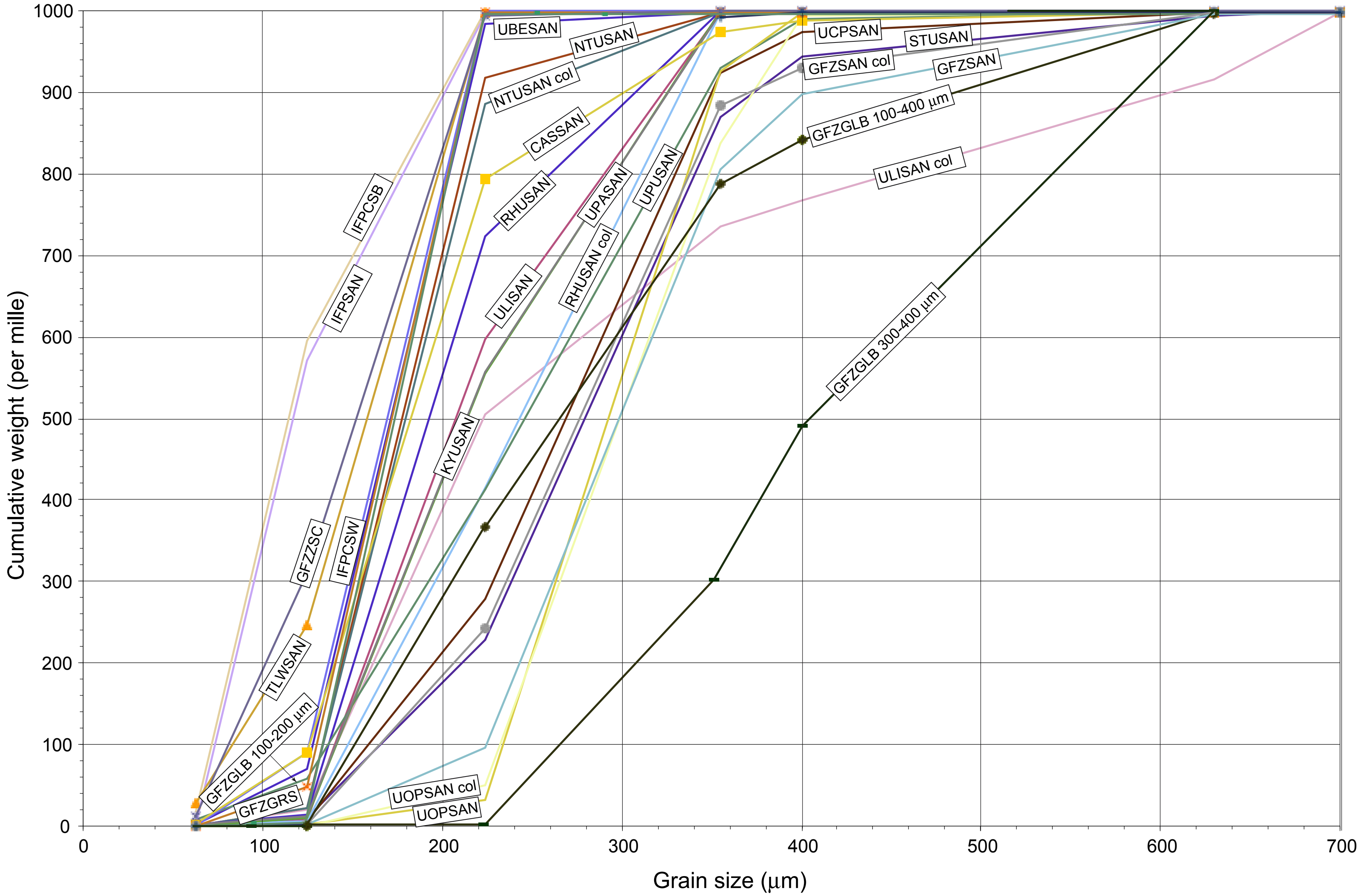

Fig. 2. Grain size classes plotted against cumulative weight.

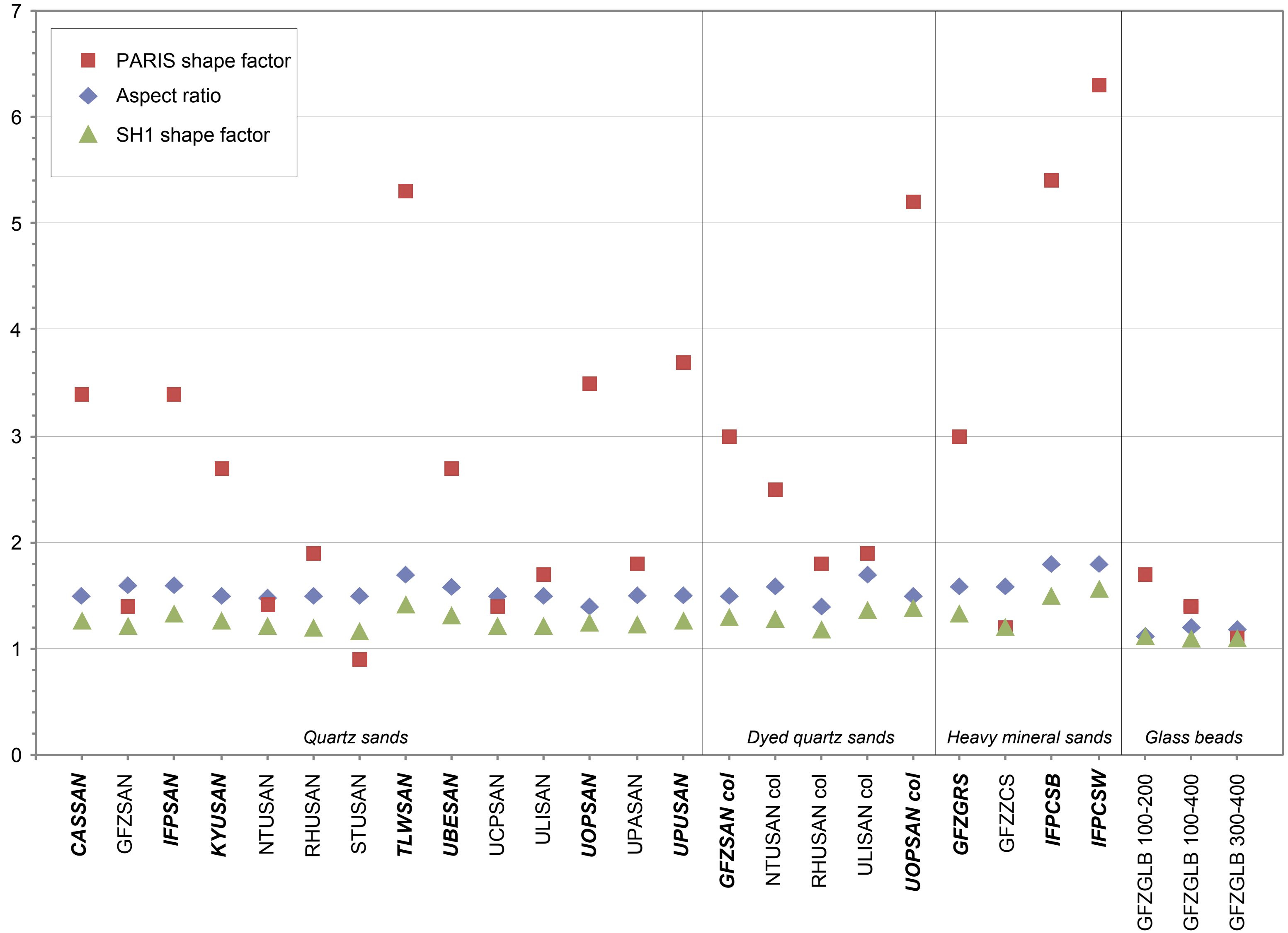

Fig. 3. Grain shape analysis using aspect ratio, and SH1 shape and PARIS factors. Angular granular materials are indicated in bold italics, rounded materials in normal font.

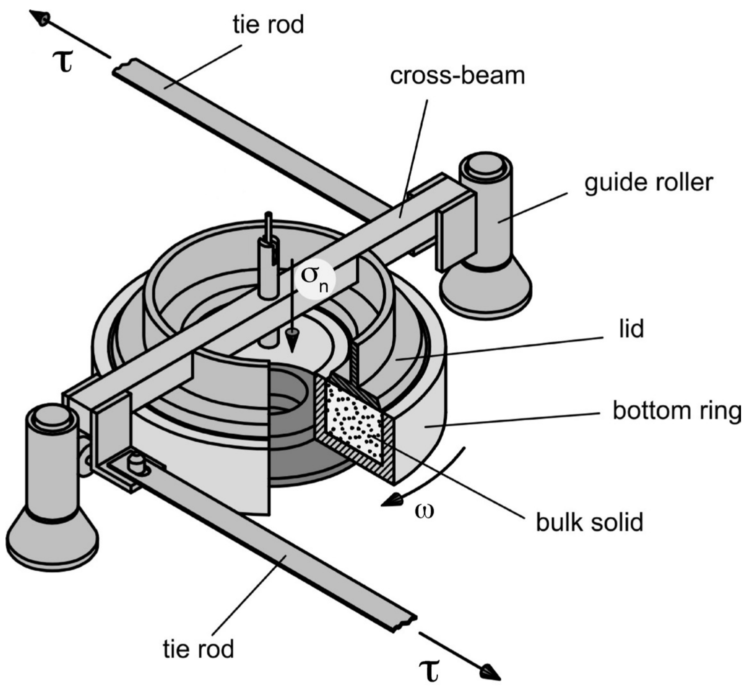

Fig. 4. Ring-shear tester (after Schulze, 1994).

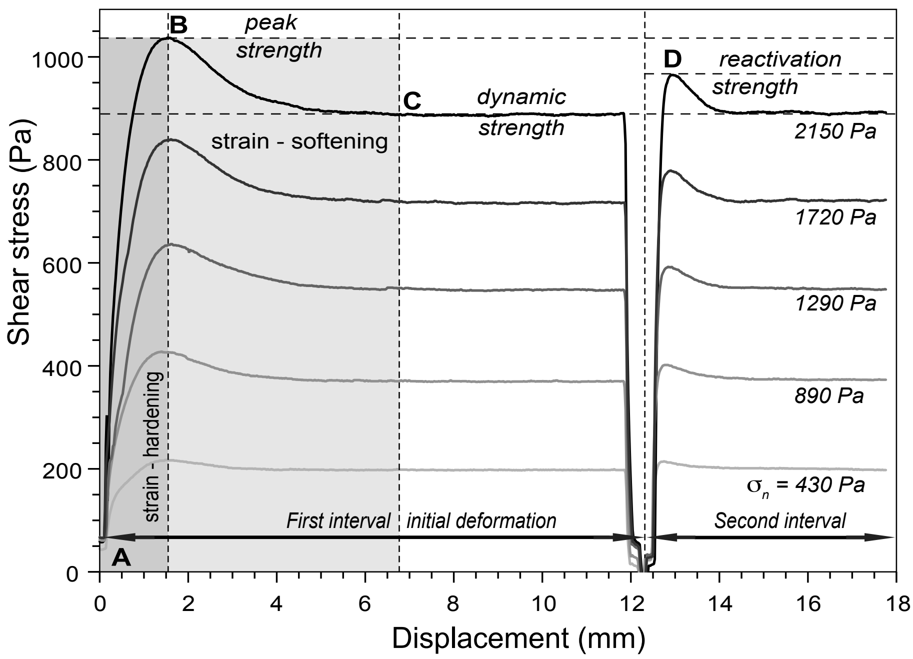

Fig. 5. Example of shear stress curves at different normal loads, AB = strain hardening part of curve, BC = strain softening part of curve, B = peak strength, C = dynamic strength, and D = reactivation strength.

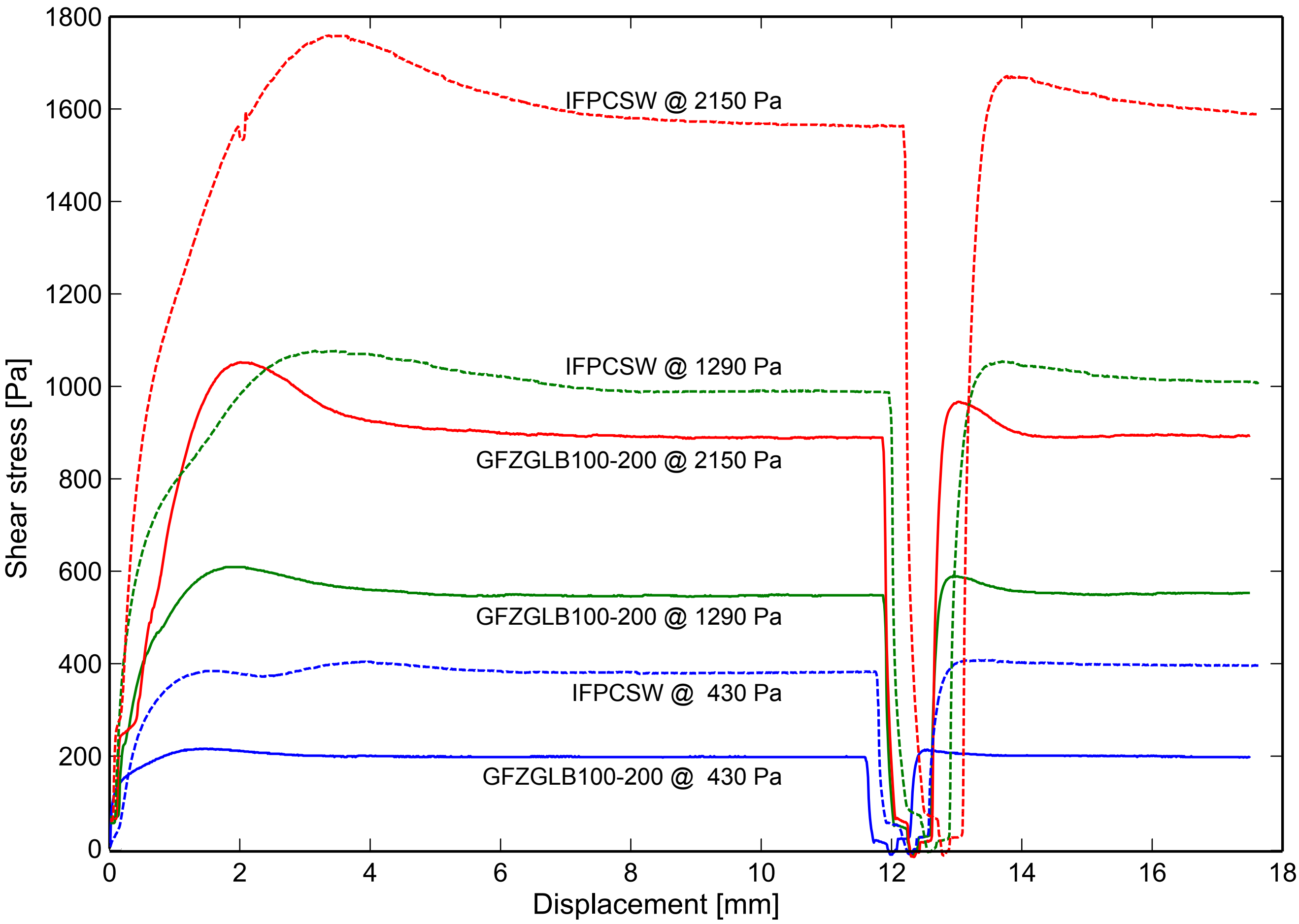

Fig. 6. Example of ring-shear test data analysis (UBESAN, internal) (a) Linear regression analysis of shear strength vs normal load data pairs (15 data). (b) Histograms of friction co-efficients and cohesion derived from mutual two-point regression analysis (90 data).

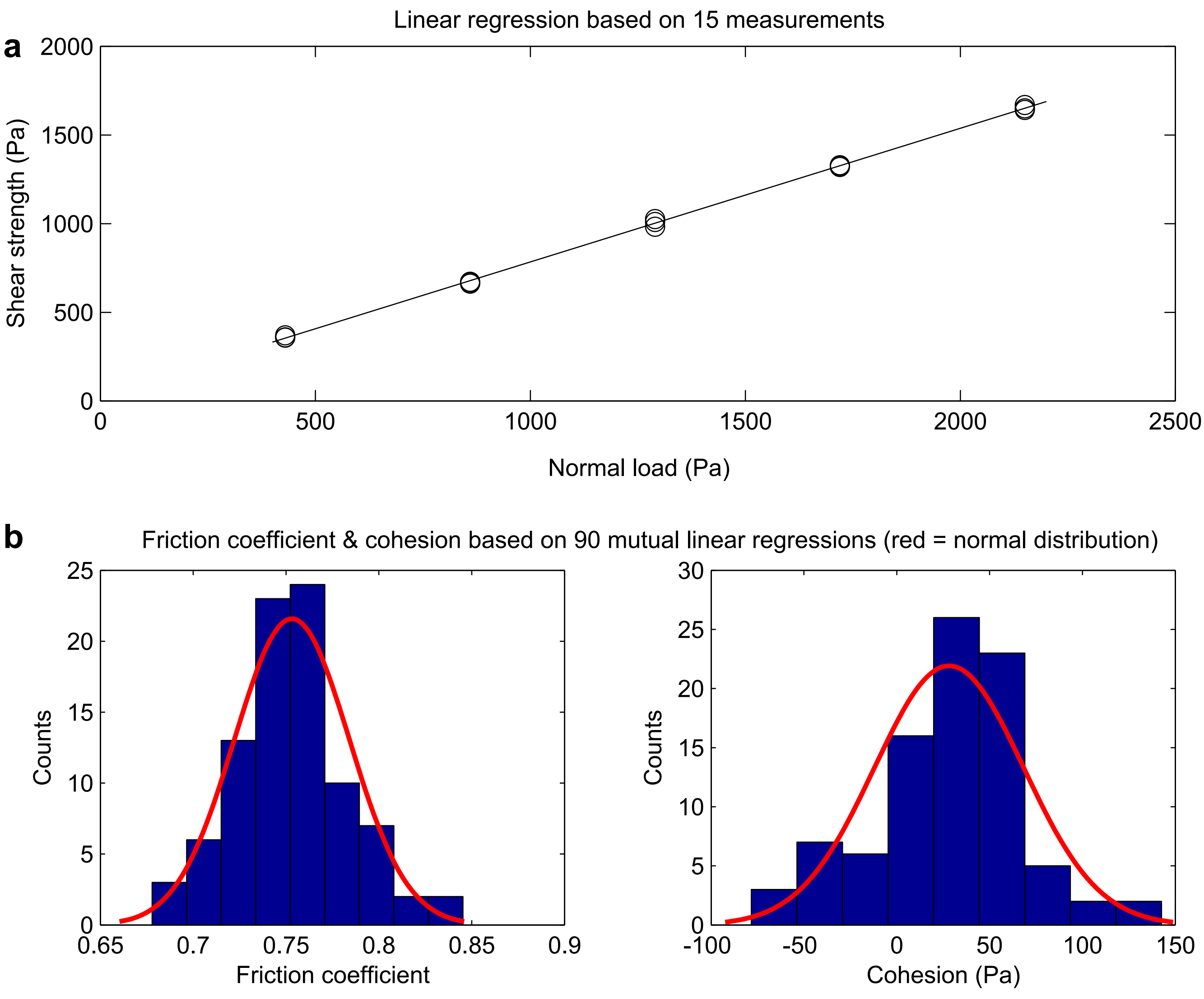

Fig. 7. Shear stress plotted as a function of cell displacement (~ the amount of shear strain) for angular quartz sand (IFPCSW) and well-rounded glass beads (GFZGLB 100-200 µm) for three different normal loads.

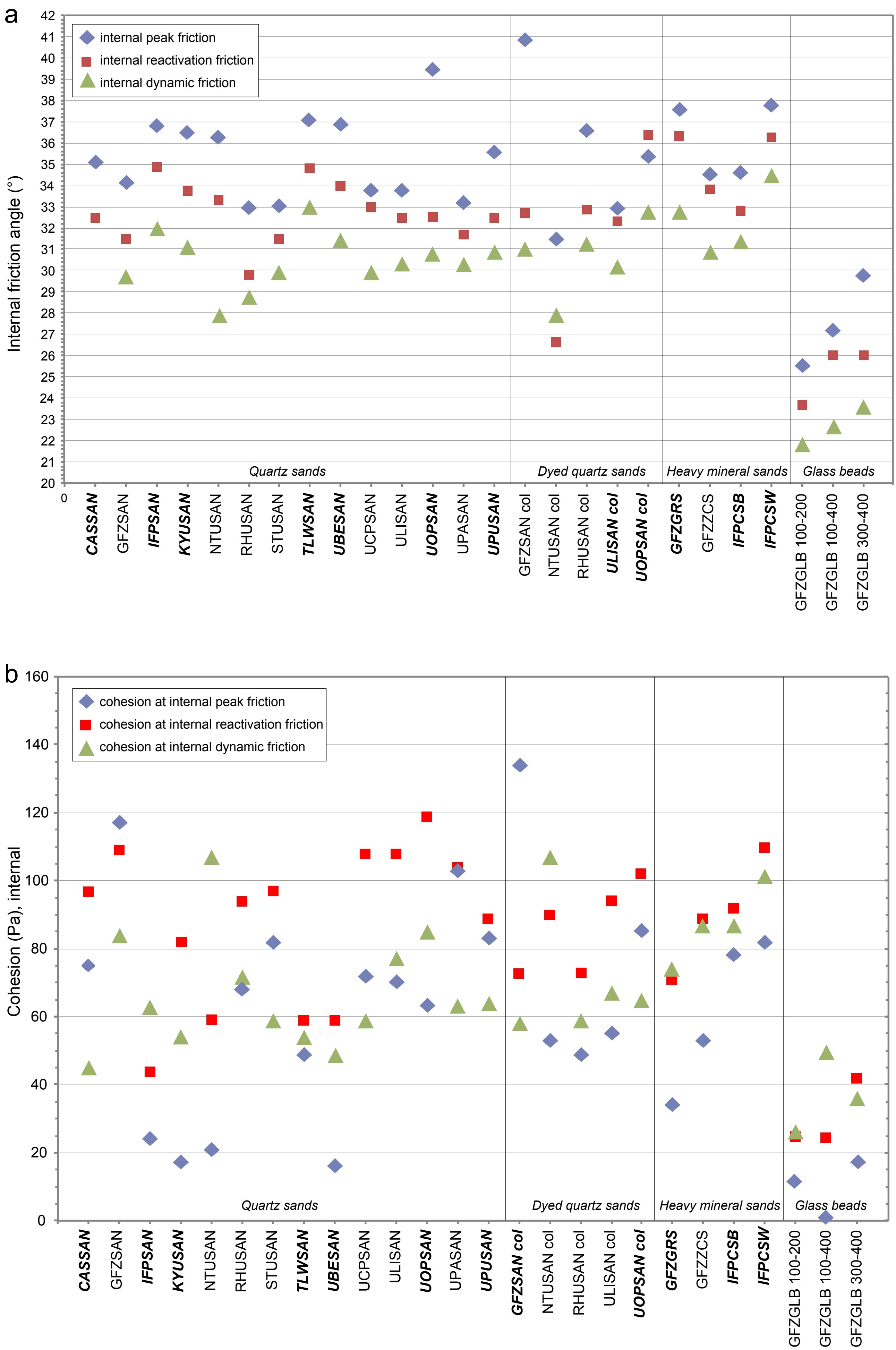

Fig. 8. Internal friction angles and cohesion values (a) Angles of internal peak friction, internal reactivation friction and internal dynamic friction. (b) Extrapolated cohesion values at internal peak friction, internal reactivation friction and internal dynamic friction. Angular granular materials are indicated in bold italics, rounded materials in normal font.

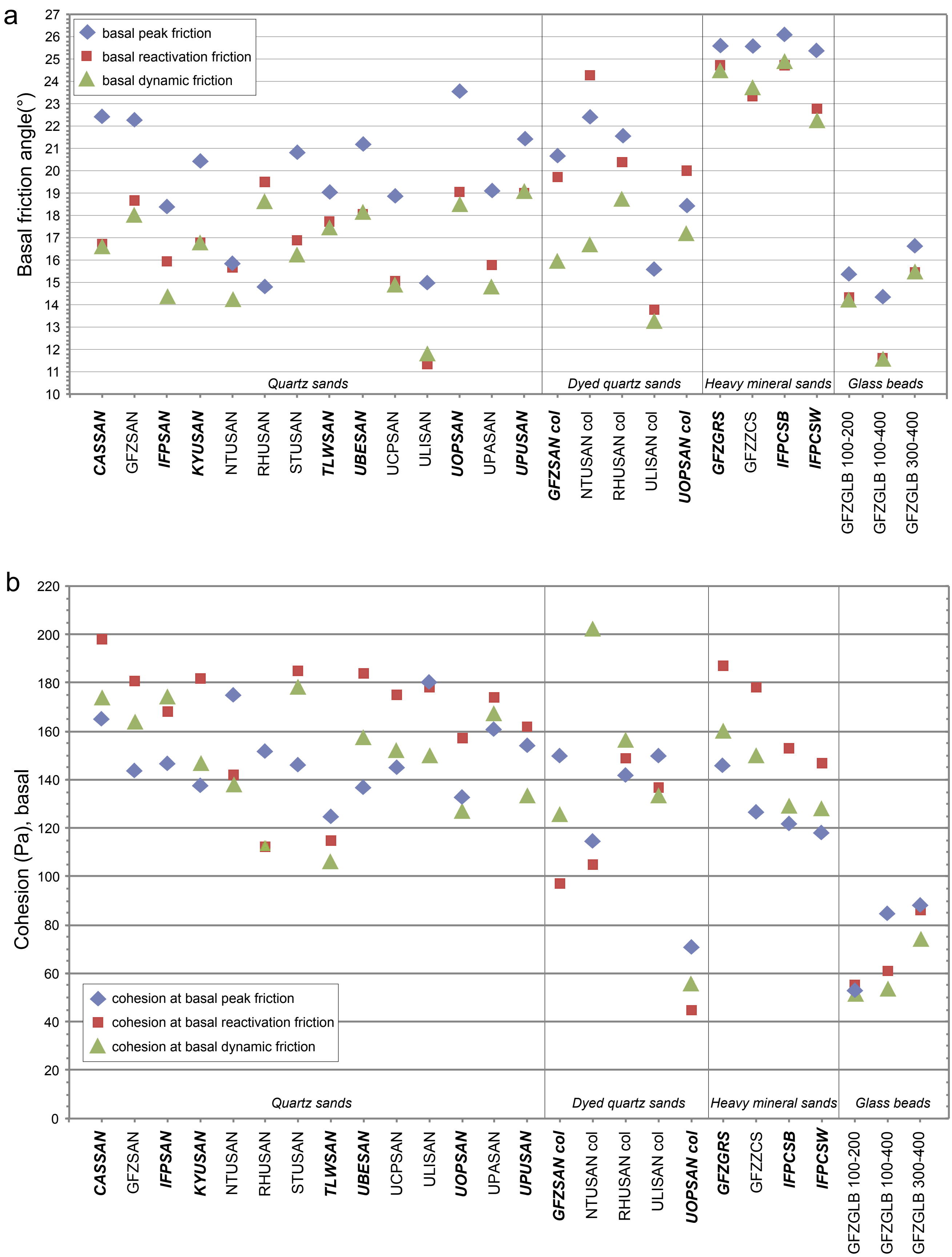

Fig. 9. Basal friction angles and cohesion values (a) Angles of basal peak friction, basal re-activation friction and basal dynamic friction. (b) Extrapolated cohesion values at basal peak friction, basal reactivation friction and basal dynamic friction. Angular granular materials are indicated in bold italics, rounded materials in normal font.

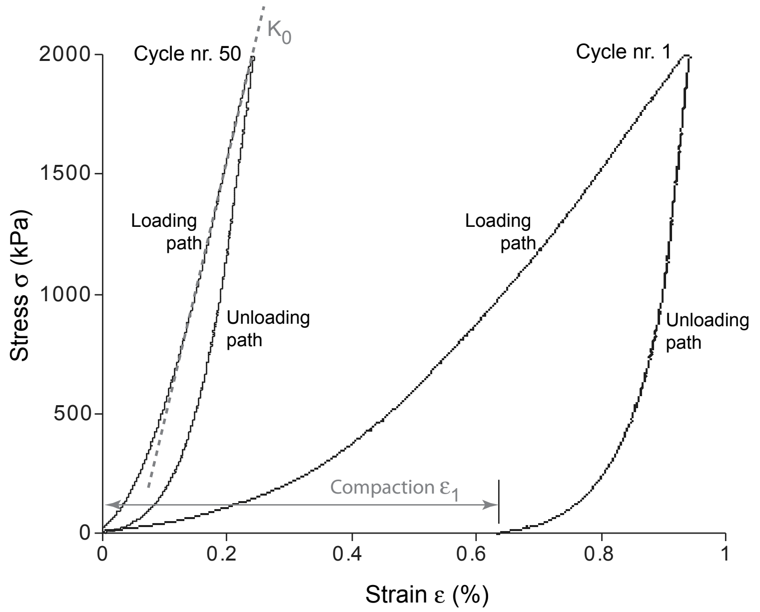

Fig. 10. Uniaxial confined compression test after the first and 50th cycle. First loading – unloading cycle is dominated by compaction; later cycles represent more elastic behaviour. The elastic modulus, K_0, is determined at the 50th cycle along loading path (dashed line).

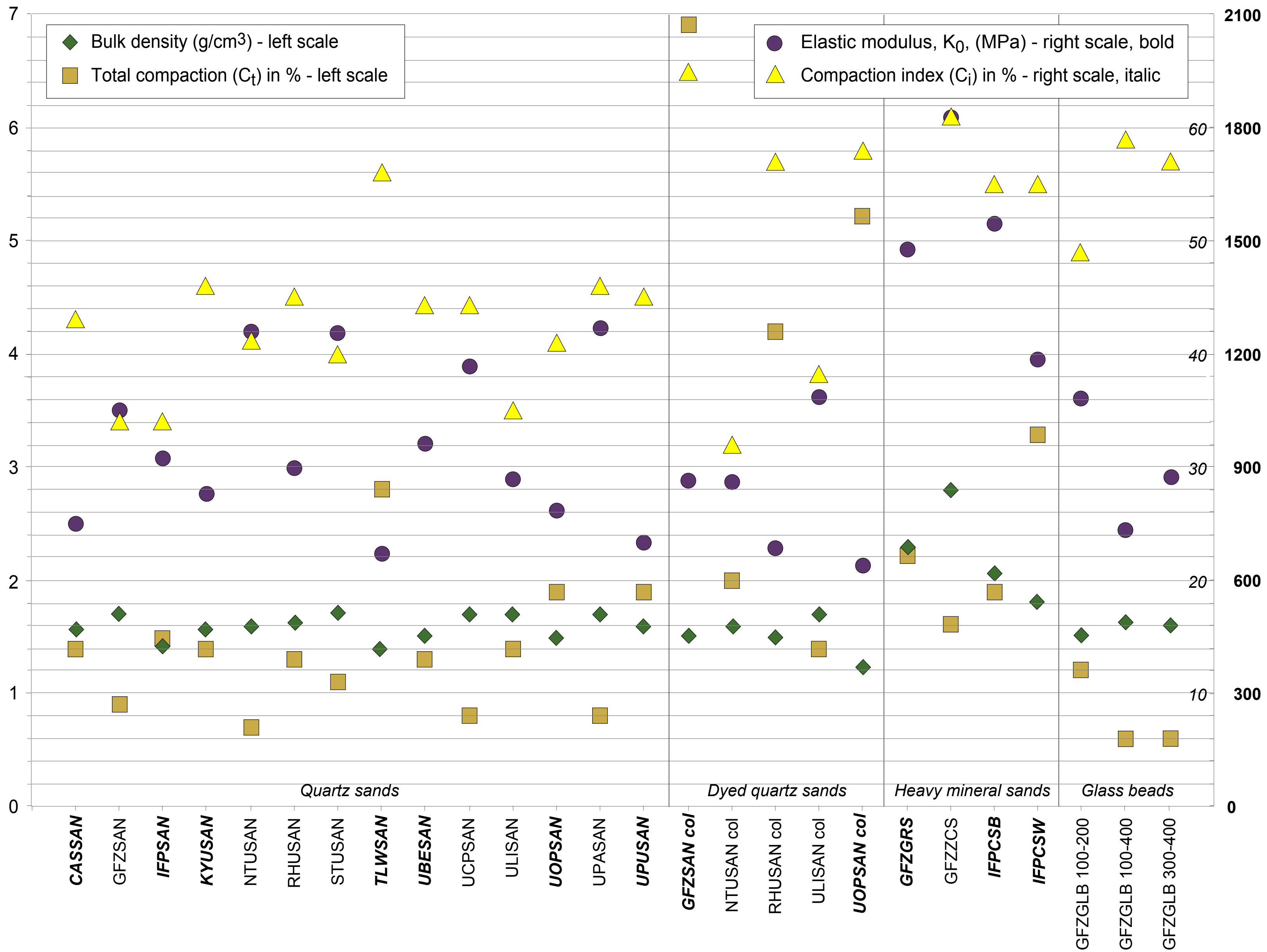

Fig. 11. Values of bulk density, compaction index (left scale), total compaction and elastic modulus, K_0, (right scale). Angular granular materials are indicated in bold italics, rounded materials

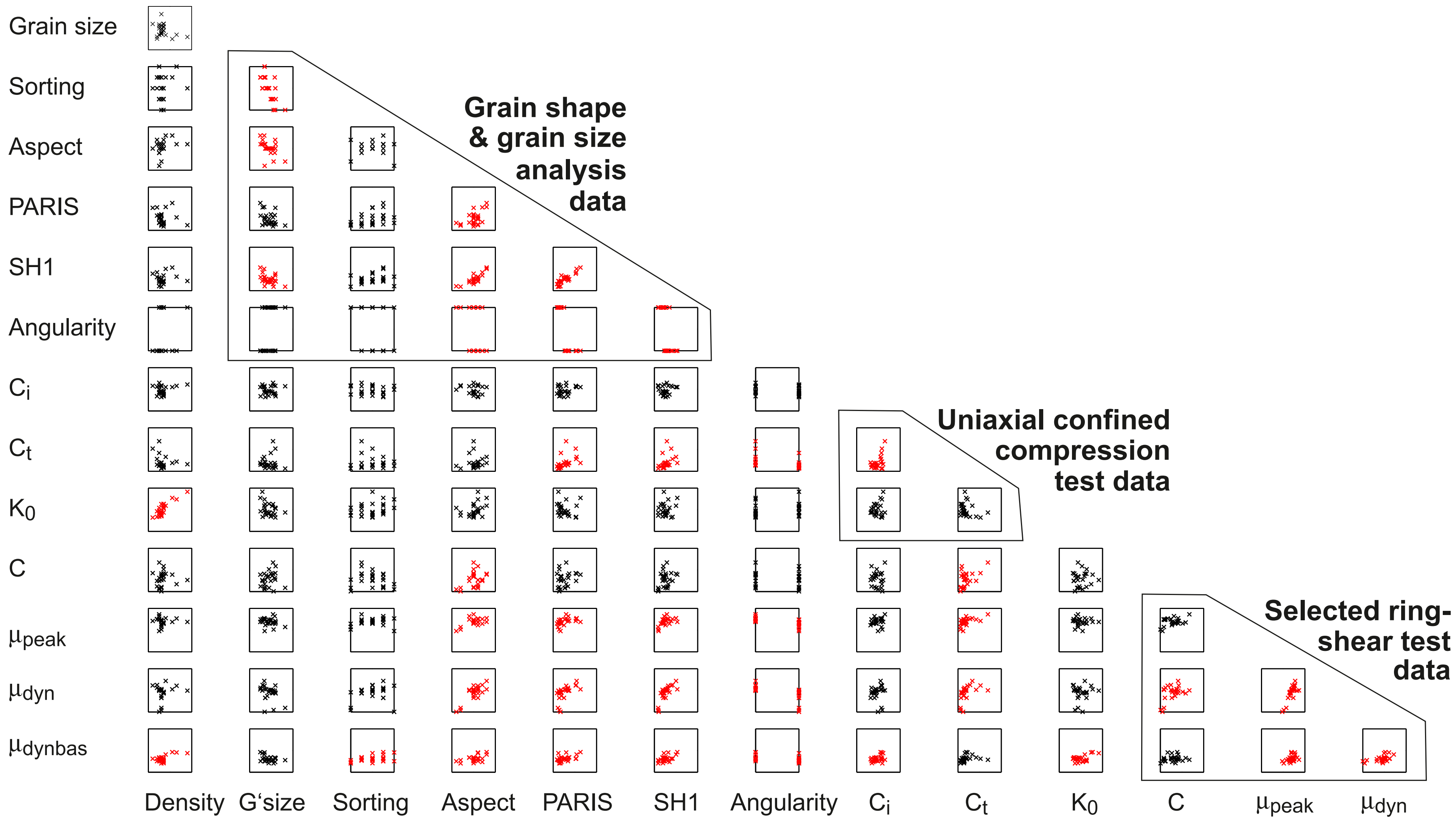

Fig. 12. Bivariate cross-correlation matrix of selected data. Points are plotted in red if the correlation is significant at the 95% level based on Pearson correlation coefficient. Apart from correlations within generic groups (shape and grain size analysis, uniaxial confined compression tests and ring shear test data), relevant and interpretable correlations exist be-tween shape parameters and friction parameters as well as between K0 with density and total compaction with internal friction. C is cohesion, C_i is compaction index, C_t is total compaction, K_0 is the elastic modulus, μ is coefficient of friction with subscripts "peak", "dyn" and dynbas" indicating coefficients of peak internal friction, dynamic internal friction and dynamic basal friction, respectively.

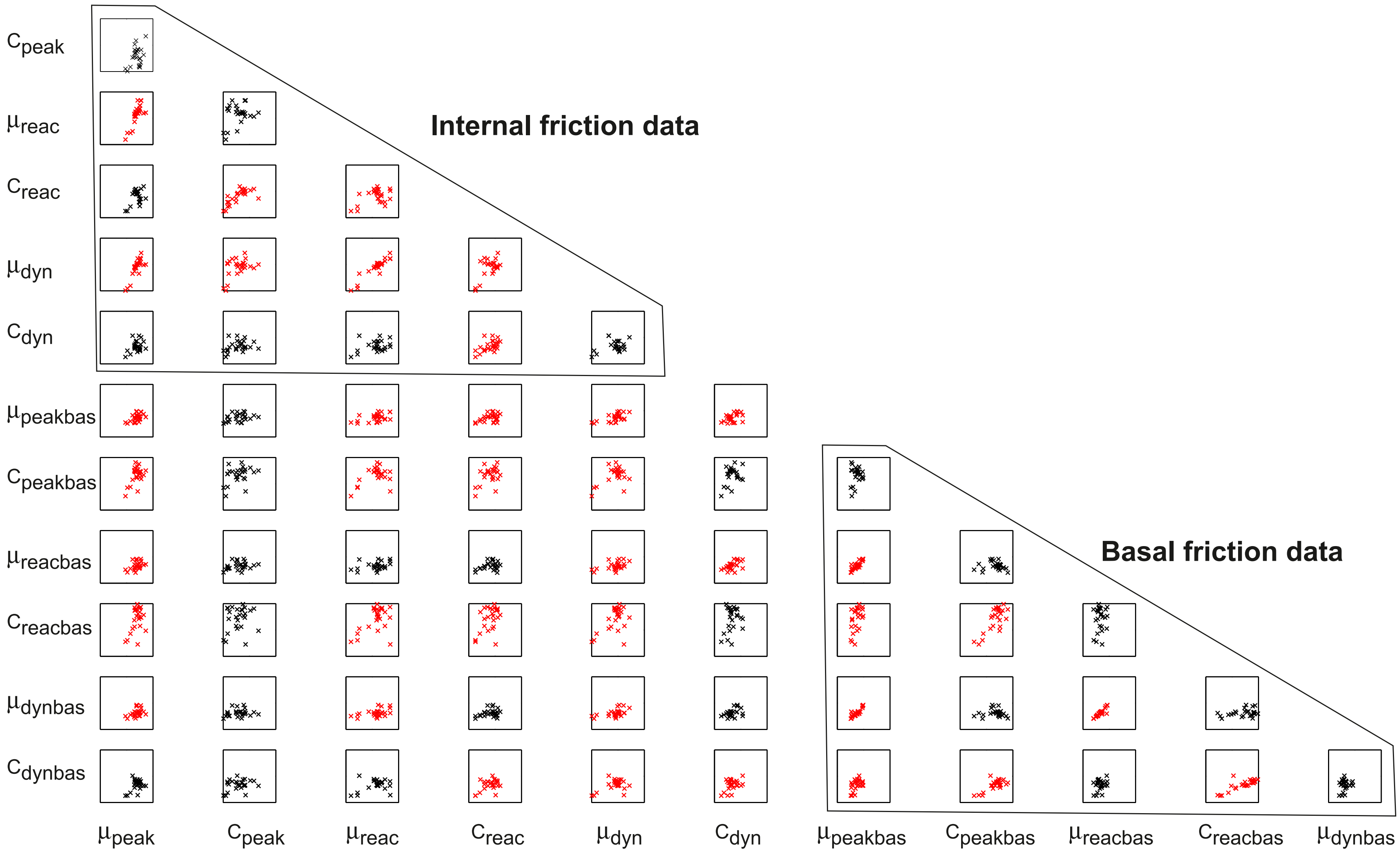

Appendix 1. Bivariate cross-correlation matrix of internal and basal friction data. C is cohesion, μ is coefficient of friction; subscripts "peak", "reac" and "dyn" indicate respective values at internal peak, internal reactivation and internal dynamic conditions, respectively; subscripts "peakbas", "reacbas" and "dynbas" indicate respective values at basal peak, basal reactivation and basal dynamic conditions, respectively.